Available online at www.sciencedirect.com
ScienceDirect
Journal of Luminescence 128 (2008) 559–564
JOURNAL OF LUMINESCENCE
www.elsevier.com/locate/jlumin

Luminescence enhancement in bromine and samarium co-doped TiO_2 semiconductor nanocrystalline powders

Chunmei Gao[a,b], Hongwei Song[a,b,*], Lanying Hu[a,b], Guohui Pan[a,b], Ruifei Qin[a,b], Fang Wang[a,b], Qilin Dai[a,b], Libo Fan[a,b], Lina Liu[a,b], Huihui Liu[a,b]

[a]*Key Laboratory of Excited State Physics, Changchun Institute of Optics, Fine Mechanics and Physics, Chinese Academy of Sciences, 16 Eastern Nan-Hu Road, Changchun 130033, PR China*
[b]*Graduate School of Chinese Academy of Sciences, 16 Eastern Nan-Hu Road, Changchun 130033, PR China*

Received 29 April 2007; received in revised form 12 July 2007; accepted 17 July 2007
Available online 18 September 2007

Abstract

In this paper, TiO_2:Sm^{3+} (0.75 mol%) nanoparticles doped with different amounts of Br^- were prepared by an improved sol–gel method and were characterized by means of X-ray diffraction (XRD), scanning electron microscopy (SEM), VG ESCALAB MKIIX-ray photoelectron spectrometer (XPS) and ultraviolet–visible diffuse reflectance spectroscopy (UV–vis DRS). Their photoluminescence (PL) properties were investigated at room temperature. The emissions of $^4G_{5/2}$–^6H_J ($J = 5/2, 7/2, 9/2$) transitions of Sm^{3+} ions were observed under the excitation wavelength at 350 nm and the emission intensity depended strongly on the doping amount of Br^-. TiO_2:Sm^{3+} (0.75 mol%) nanoparticles doped with 1 mol% of Br^- calcined at 700 °C exhibit highest intensity of luminescence, which is nearly three times than the undoped one. The mechanism of photoluminescence in the co-doped system was discussed.

Keywords: TiO_2; Samarium; Bromine; Luminescence

1. Introduction

Titanium oxide (TiO_2) is an important metal-oxide semiconductor with relatively wide band gaps (3.0 eV for rutile and 3.2 eV for anatase), high refractive indices ($n = 2.52$ for anatase phase and $n = 2.76$ for rutile phase) and lower phonon energy ($<700\,cm^{-1}$), which show interesting variations influenced by oxygen defects, impurities and crystalline modifications. A number of investigations have focused on semiconductor photocatalysis for their application in solar energy conversion and environmental purification, since Fujishima and Honda discovered the photocatalytic splitting of water on the TiO_2 electrodes in 1972 [1–5]. As reported in the literatures, transition metals doping (e.g., Co, Fe) [6,7], non-metallic elements doping (e.g., N, C, S) [8,9] and rare earth ions doping (e.g., Nd, La, Ce) [10–13] have led to noticeable improvement of the photocatalytic activity of TiO_2 in the visible region.

There are certain intrinsic relationships between the luminescence spectrum and photocatalytic activity of a semiconductor material according to the mechanisms of luminescence and photocatalysis. And, luminescence spectrum is an effective way to study the electronic structure, optical and photochemical properties of semiconductor materials, by which the information such as surface oxygen vacancies (SOVs) and defects, as well as the efficiency of charge carrier trapping, immigration and transfer can be obtained [14–17]. In some rare earth doped TiO_2, exciting the TiO_2 in its band gap results in energy transfer to the emitting states of rare earth ions, and it is possible to observe luminescence from some kind of the rare earth ions. Various rare earth ions (Sm^{3+} [18], Er^{3+} [19], Eu^{3+} [20], Tb^{3+} [21]) have previously been incorporated into sol–gel prepared TiO_2 and their optical properties have been studied. Kiisk et al. [18,22,23] prepared a set of

*Corresponding author. Key Laboratory of Excited State Physics, Changchun Institute of Optics, Fine Mechanics and Physics, Chinese Academy of Sciences, 16 Eastern Nan-Hu Road, Changchun 130033, PR China. Fax: +86 431 86176320.
E-mail address: hwsong2005@yahoo.com.cn (H. Song).

0022-2313/$ - see front matter © 2007 Elsevier B.V. All rights reserved.
doi:10.1016/j.jlumin.2007.07.020

Sm-doped TiO_2 thin films by sol–gel method and discussed relaxation of electronic excitations and the energy transfer process to Sm^{3+} ions. Our group has synthesized samarium and metal ions co-doped TiO_2 semiconductor by the sol–gel method. It is believed that co-doped TiO_2:Sm^{3+} can be a candidate to increase the photoluminescence (PL) intensity and to discuss the PL and energy transfer mechanism.

In this study, Br^- anion and Sm^{3+} ion co-doped TiO_2 nanocrystals were prepared by an improved sol–gel method and their PL properties were studied. It is observed that co-doping of Br^- ions remarkably influences PL properties of TiO_2:Sm^{3+}.

2. Experimental details

2.1. Synthesis of the samples

Samples of Br^- and Sm^{3+} co-doped TiO_2 were prepared by sol–gel method using $Ti(OC_4H_9)_4$ ($Ti(OBu)_4$), $Sm(NO_3)_3$ and NH_4Br as raw materials. The TiO_2 sol was obtained by the following: 20 ml of $Ti(OC_4H_9)_4$ and 0.02 g sodium laurylsulfonate ($CH_3(CH_2)_{10}CH_2SO_3Na$) was dissolved in 40 ml of ethyl alcohol(C_2H_5OH), forming the solution of precursor. Secondly, the mixture of 20 ml of ethyl alcohol, 2 ml of acetic acid (CH_3COOH), a certain amount of NH_4Br, a certain amount of $Sm(NO_3)_3$ and 4 ml of deionized water were mixed dropwise into the precursor solution under magnetic stirring at room temperature. The molar ratio of $Ti(OC_4H_9)_4$:$Sm(NO_3)_3$:NH_4Br was 100:0.75:x ($x=0$, 1, 2, 3, 5). The mixture was hydrolyzed at room temperature for 40 min under vigorous stirring, and the transparent sol was obtained. The gel was prepared by aging the sol for 48 h at room temperature. The derived gel was dried at 100 °C for 24 h to remove the solvents. Then the gels were annealed at 500, 550, 600, 650 and 700 °C for 2 h after grinding.

2.2. Characterization of the samples

X-ray diffraction patterns (XRD) were obtained on a Rigaku D/max-rA powder diffractometer with Cu Kα ($\lambda=1.54078$ Å) radiation. TEM images were taken on a JEM-2010 transmission electron micrograph under a working voltage of 200 kV. The surface compositions and chemical states of the samples were examined by a VG ESCALAB MKIIX-ray photoelectron spectrometer (XPS) using a monochromatic aluminum X-ray source. The pressure was maintained at 6.3×10^{-5} Pa. The binding energies were calibrated with respect to the signal for adventitious carbon (binding energy = 284.6 eV). UV–vis absorption spectra of TiO_2 powders were obtained for the dry pressed disk samples using a UV–vis spectrophotometer Cary 100 Scan Spectrophotometers. Absorption spectra were referenced to $BaSO_4$. Emission spectra at room temperature were measured with a Hitachi F-4500 fluorescence spectrometer. In the measurements of fluorescence dynamics, a 350-nm light generated from the Fourth-Harmonic Generator pumped by the pulsed Nd:YAG laser was used as excitation source. It is with a line width of 1.0 cm^{-1}, pulse duration of 10 ns and repetition frequency of 10 Hz. The spectra were recorded by a Spex-1403 spectrometer, a photomultiplier and a boxcar integrator and processed by a computer.

3. Results and discussion

3.1. Crystal structure and morphology

Fig. 1 shows the XRD patterns of TiO_2:Sm^{3+} (a) and TiO_2:Sm^{3+} doped with 1 mol% of Br^- (b) nanoparticles calcined at different temperatures. The XRD peaks at $2\theta=25.25^\circ$ (1 0 1) in the spectrum of TiO_2 are easily identified as the crystal of anatase form, whereas the XRD peaks at $2\theta=27.42^\circ$ (1 1 0) are easily taken as the crystal of rutile form. The XRD intensities of the anatase (1 0 1) peak and the rutile (1 1 0) peak were also analyzed. In the figure, all the diffraction lines are assigned to tetragonal phase of anatase calcined at 500 and 600 °C. Then the rutile phase began to appear when calcining temperature was 650 °C and the anatase phase disappeared at 700 °C for both pure and Br-doped TiO_2:Sm^{3+} nanoparticles. XRD patterns of TiO_2:Sm^{3+}/Br^- were similar to that of TiO_2:Sm^{3+}. No additional diffraction lines were observed, suggesting that Br^- ions were doped into the TiO_2 lattices. In addition, the co-doping of Br^- has a little influence on widths of XRD patterns and the evaluated results show that the weight percentage of anatase becomes lower in the case of co-doping. Estimated by diffraction peak of (1 0 1) using Scherrer equation, the crystalline sizes for the samples TiO_2:Sm^{3+} and TiO_2:Sm^{3+}/Br^- were determined to be 12 and 18 nm, respectively. Hence, we believe that the Br^- dopant not only could promote the phase transformation

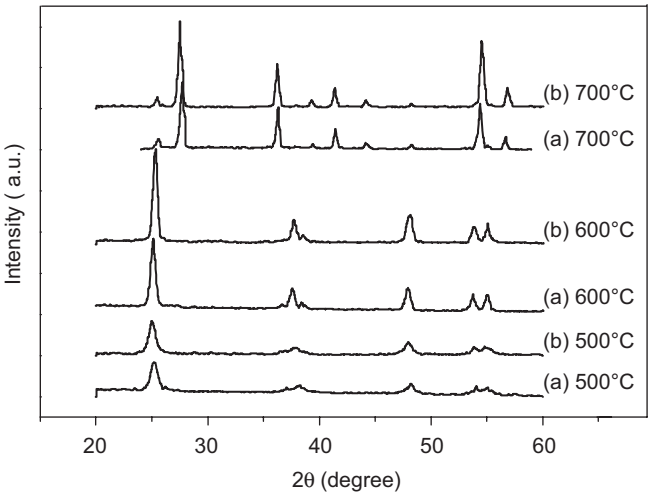

Fig. 1. XRD patterns of TiO_2:Sm^{3+} (0.75 mol%) nanoparticles (a) and TiO_2:Sm^{3+} (0.75 mol%)/Br^- (1 mol%) nanoparticles (b) by respective thermal treatment at 500, 600 and 700 °C.

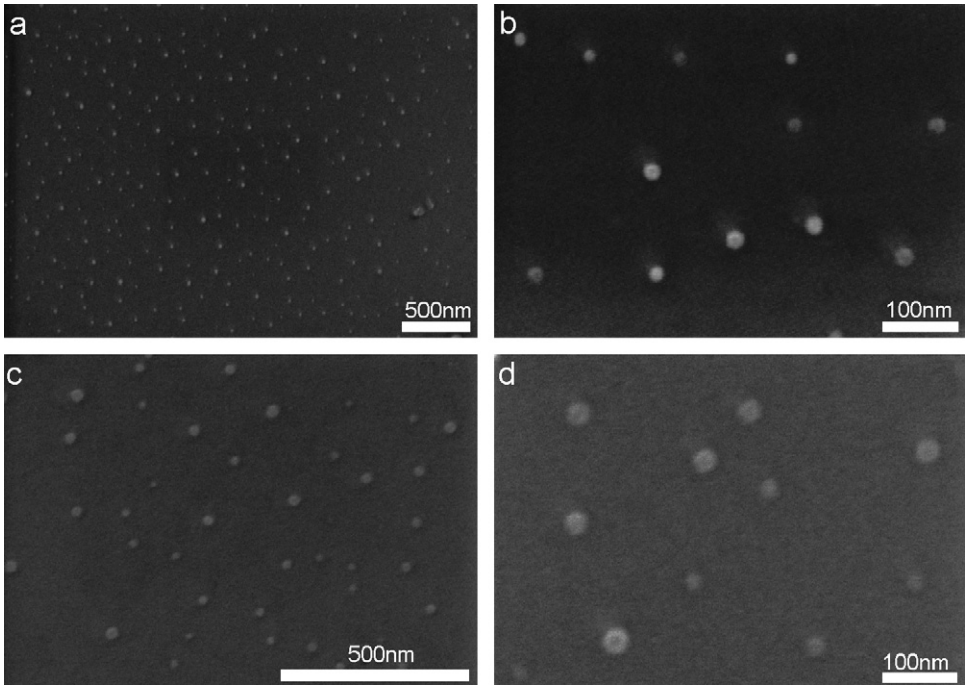

Fig. 2. TEM photographs of pure (a and b) and 1 mol% of Br^--doped (c and d) $TiO_2:Sm^{3+}$ (0.75 mol%) nanoparticles calcined at 700 °C.

from anatase to rutile but also enhance the increase of $TiO_2:Sm^{3+}$ particle size.

Fig. 2 shows the TEM photographs of pure (a) and 1 mol% of Br^--doped (b) $TiO_2:Sm^{3+}$ nanoparticles calcined at 700 °C. It can be found that the pure and 1 mol% of Br^--doped $TiO_2:Sm^{3+}$ nanoparticles calcined at 700 °C both yield nanospheres, with average particle size of ~20 and ~25 nm, respectively. The average grain size determined from TEM image is a little bit larger than that determined from the Scherrer equation. This is because the size distribution in the system is inhomogeneous and smaller nanograins contribute more to the broadening of the diffraction peaks. Moreover, the XRD and TEM images both show that the average particle size for the nanocrystals co-doped with Br^- ions becomes larger in comparison to $TiO_2:Sm^{3+}$, implying that the Br^--doping can accelerate the increase of $TiO_2:Sm^{3+}$ particle.

The XPS spectra of Br^--doped $TiO_2:Sm^{3+}$ by thermal treatment at 700 °C are depicted in Fig. 3. Sharp and symmetrical XPS peaks are observed at about 1110, 458.6, 281 and 69 eV, corresponding to Sm_{3d}, Ti_{2p}, C_{1s} and Br_{3d}, respectively. The main chemical states of Sm, Br and Ti in the samples are +3, −1 and +4 valence, respectively. The C element is ascribed to the residual carbon from precursor solution and the adventitious hydrocarbon from the XPS instrument itself. The O_{1s} peak positions are at about 530 eV. The enlarged spectrum indicates that there are at least two kinds of chemical states according to the binding energy range from 528 to 533 eV, including crystal lattice oxygen (O_L) and adsorbed oxygen (O_H). The binding energies of O_L and O_H are 529.9 and 531.6 eV, respectively. The O_L XPS is mainly attributed to the contribution of Ti–O in TiO_2 crystal lattice, and the O_H XPS is closely related to the hydroxyl groups resulting from the chemisorbed water.

For a careful XPS analysis, the evaluated data of atomic number ratio and relative SOVs content are given in Table 1, which show that the percentages of SOV content of undoped and Br-doped $TiO_2:Sm^{3+}$ nanoparticles are 1 and 14, respectively, demonstrating that the SOV content of $TiO_2:Sm^{3+}$ is greatly enhanced by co-doping of Br^-. It is suggested that Br^- come into the TiO_2 lattices substituting for O^{2-}. Br^- possibly exists as the main chemical bonds of Ti–Br, because in the preparation NH_4Br is easy to decompose into NH_3 and HBr in water and form chemical bonds of Ti–Br and O–H during the process of thermal treatment.

3.2. Optical absorption and characteristic luminescence

Br^--doping obviously affects light absorption characteristics of $TiO_2:Sm^{3+}$, as shown in Fig. 4. According to the energy band structure of TiO_2, the optical absorption being shorter than 400 nm is mainly attributed to the electron transitions from the valence band to the conduction band (band-to-band transition, O_{2p}–Ti_{3d}), while the weak optical absorption being longer than 400 nm results from exciton transitions closely related to the SOV and defects. The luminescence excitation spectra of $TiO_2:Sm^{3+}$ exhibits an intense broad band centered at 350 nm (3.4 eV), which is assigned to titania host absorption, confirming the effective energy transfer from TiO_2 host to Sm^{3+} ions. The excitation spectra of the Br^--doped $TiO_2:Sm^{3+}$ samples show stronger absorption in the UV–vis range and a red

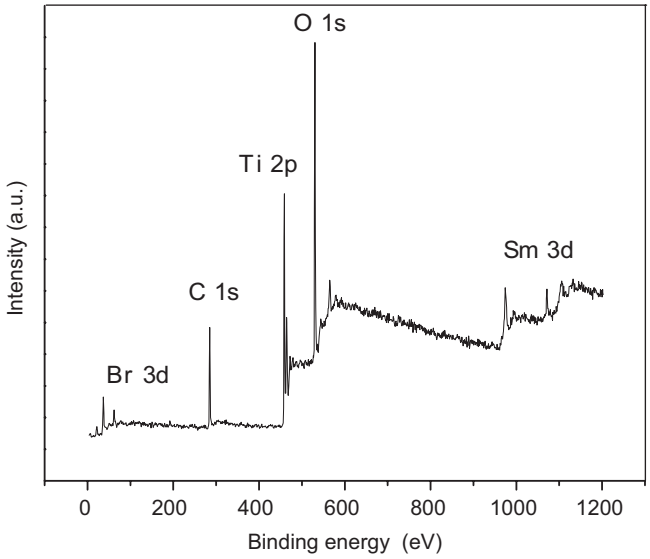

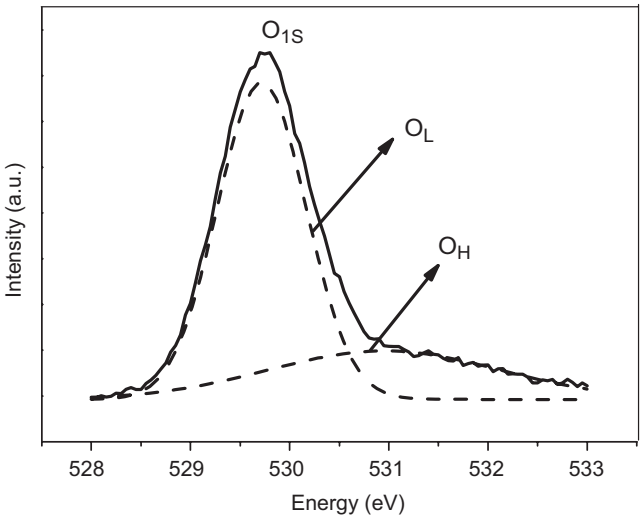

Fig. 3. XPS spectra of 1 mol% of Br-doped TiO_2:Sm^{3+} (0.75 mol%) nanoparticles by thermal treatment at 700 °C.

Table 1
Atomic number ratio of O_L, Ti, Sm and Br and the SOV content of pure (a) and 1 mol% of Br-doped (b) TiO_2:Sm (0.75 mol%) nanoparticles calcined at 700 °C

Sample	Atomic number ratio of O_L, Ti, Sm and Br	SOV content (%)
(a)	100:50.3:0.4:0	1
(b)	100:58.0:0.4:0.5	14

shift in the photocatalytic reaction, which is attributed to the increase in the SOV amount [24].

The co-doping of Br^- has influence not only on location of excitation band, but also on the fluorescence intensity and dynamics. Fig. 5 shows the PL spectra of pure and different amounts of Br^--doped TiO_2:Sm^{3+} nanoparticles calcined at 700 °C. The PL emission spectra of the samples show emission band at 582, 610 and 660 nm, and they are

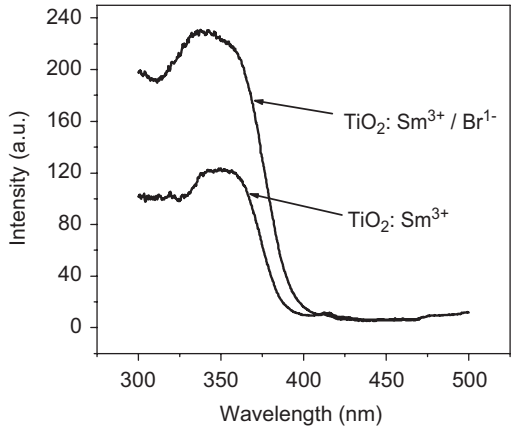

Fig. 4. Excitation spectra of pure and 1 mol% of Br^--doped TiO_2:Sm^{3+} (0.75 mol%) powders prepared by thermal treatment at 700 °C.

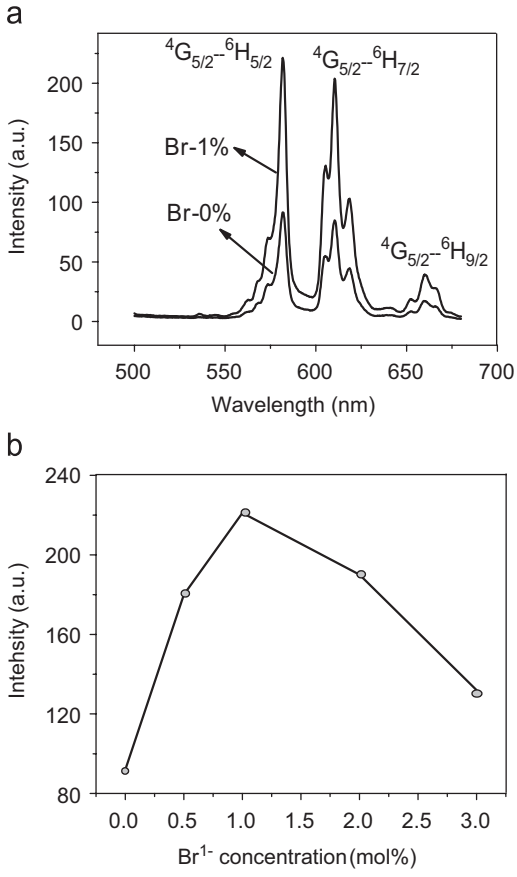

Fig. 5. (a) Emission spectra of different amounts of Br^--doped TiO_2:Sm^{3+} (0.75 mol%) ($\lambda_{ex} = 350$ nm) and (b) emission intensity of Br^--doped TiO_2:Sm^{3+} (0.75 mol%) nanocrystals as a function of Br^- concentration.

assigned to the electronic transition of $^4G_{5/2}$–$^6H_{5/2}$, $^4G_{5/2}$–$^6H_{7/2}$ and $^4G_{5/2}$–$^6H_{9/2}$ of Sm^{3+}, respectively. In comparison to the pure complex, the intensity of TiO_2:Sm^{3+} nanoparticles increases. The fine structure can be explained by taking into account that the ^6H_J levels are split into $2J+1$ sublevels in the crystal field. Although the radii of

RE ions seem to be too large to allow them to replace Ti^{4+} in an anatase crystal (1.04 Å versus 0.64 Å), the well-resolved ^6H_J levels clearly demonstrate that Sm^{3+} ions are fitted into a quite regular environment, contrary to the situation encountered in amorphous matrices. It is reasonable to conclude that the Sm^{3+} ion distorts the TiO_6 octahedron substituting the Ti^{4+} ion in shifted position [12,25]. It can be found that pure and Br^--doped TiO_2:Sm^{3+} nanoparticles exhibit similar PL, demonstrating that Br^--doping does not result into new PL.

Based on the model given by Frindell and Bartl [26], a modified model for the energy transfer in this co-doping system is proposed in Fig. 6. In Fig. 6, (1) is the generation process of excitons, (2) is the non-radiative energy transfer process from an exciton to defect I, (3) is the non-radiative energy transfer process from defect I to Sm^{3+}, (4) is the emission process of Sm^{3+} and (5) is the non-radiative transition from excited Sm^{3+} to defect II. In the model, defect I is attributed to the defect level caused by the TiO_2 host. According to the result of XPS, it may be related to oxygen vacancy. Defect II is attributed to the level depending on Br-doping. On one hand, the doping of Br^- leads to the amount increase of oxygen vacancies in the TiO_2:Sm^{3+} nanoparticles, which bridges the energy transfer from the exciton to the Sm^{3+} more effectively. As a consequence, the PL of inner-shell transitions of Sm^{3+} increases. On the other hand, the doping of Br^- also leads to the amount increase of the defects related to Br^- (defect II). The non-radiative energy transfer from excited state of Sm^{3+} to defect II thus increases, leading to the decrease of emission intensity and lifetime. Therefore, an intensity maximum occurs as the concentration of Br^- varies.

To study the decay behaviors of Sm^{3+} luminescence in the TiO_2:Sm^{3+}/Br^-phosphors, the kinetic curves for the Sm^{3+} representative emission of $^4G_{5/2}$–$^6H_{7/2}$ (610 nm) were measured. The decay curves for both phosphors can be fitted into the bi-exponential function. It was attributed to the two different "types" of Sm^{3+} ions present. The Sm^{3+} ions near the surface and the interior Sm^{3+} ions. In

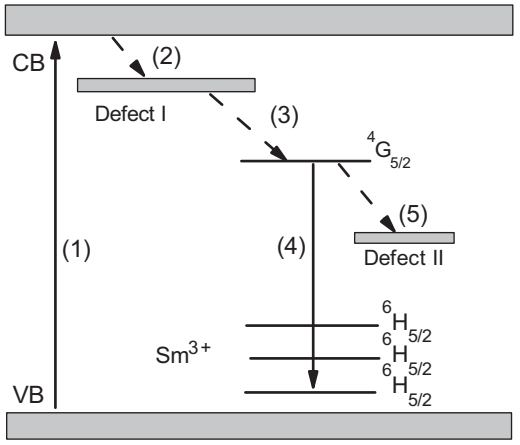

Fig. 6. Schematic of photoluminescence processes in TiO_2:Sm^{3+}, Br^- nanocrystals.

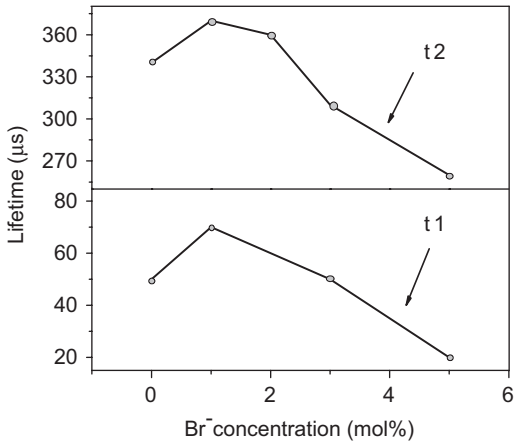

Fig. 7. Decay curves of emission from $^4G_{5/2}$ of Sm^{3+} ions to $^6H_{7/2}$ (610 nm) of different amounts of Br^--doped TiO_2:Sm^{3+} (0.75 mol%).

nanoparticles, more atoms are located in/near the particle surface, and numerous surface defects exist. These defects may increase the degree of disorder and lower the local symmetry of Sm^{3+} ions located in/near the surface of the particles. As a consequence, the radiative transition rate of $^4G_{5/2}$–$^6H_{7/2}$ increases. Thus, we get two decay time constants. The lifetime constants versus Br^- concentration in the TiO_2:Sm^{3+}/Br^- nanocrystals are drawn in Fig. 7. It can be seen that the lifetime initially increases with increased concentration, then it approaches a maximum at the concentration of 1 mol% (Br^- concentration), and then it decreases as the doping concentration increases further. The variation of fluorescence lifetime on Br^--doping can be also explained according to Fig. 6. As discussed above, the Br^--doping can lead to the amount increase of defect I, which bridges the energy transfer from the exciton to the Sm^{3+} more effectively, then the lifetime initially increases with increased concentration of Br^-. But the doping of Br^- also leads to the amount increase of defect II, which attributed to the increase of the non-radiative transition. If Br^- content continued to increase, namely more than 1 mol%, the effect of defect II dominates in the energy transfer process, thus the lifetime is decreased.

4. Conclusions

TiO_2 nanoparticles doped with different amounts of Sm^{3+} and different amounts of Br^- were prepared by an improved sol–gel method. It was observed that Br^--doping did not result in new luminescence, but in the variation of fluorescence intensity of Sm^{3+}. In nanoparticles of TiO_2:Sm^{3+} doped with 1 mol% of Br^-, the photoluminescence intensity of Sm^{3+} increased three times in contrast to the undoped one, while the fluorescence lifetime becomes a bit longer. As the content of Br^- increased continuously, the emission intensity gradually decreased and the lifetime became shorter. A model was proposed to explain the photoluminescence behavior in the Br^- co-doped TiO_2:Sm^{3+} nanoparticles.

Acknowledgments

This work is supported by the National Nature Science Foundation of China (Grants 10374086 and 10504030) and Talent Youth Foundation of JiLin Province (Grant 20040105).

References

[1] K. Honda, A. Fujishima, Nature 238 (1972) 37.
[2] A.L. Linsebigler, G. Lu, J.T. Yates Jr., Chem. Rev. 95 (1995) 735.
[3] M.R. Hoffmann, S.T. Martin, W. Choi, D.W. Bahnemann, Chem. Rev. 95 (1995) 69.
[4] Y.M. Xu, C.H. Langford, Langmuir 17 (2001) 897.
[5] J.C. Yu, W. Ho, J. Yu, H. Yip, P.K. Wong, J. Zhao, Environ. Sci. Technol. 39 (2005) 1175.
[6] H. Yamashita, M. Harada, J. Misaka, M. Takeuchi, B. Neppolian, M. Anpo, Catal. Today 84 (2003) 191.
[7] D.H. Kim, S.I. Woo, S.H. Moom, H.D. Kim, B.Y. Kim, J.H. Cho, Y.G. Joh, E.C. Kim, Solid State Commun. 136 (2005) 554.
[8] H. Kamisaka, T. Adachi, K. Yamashita, J. Chem. Phys. 123 (2005) 084704.
[9] K. Madhusudan Reddy, B. Baruwati, M. Jayalakshmi, M. Mohan Rao, S.V. Manorama, J. Solid Chem. 178 (2005) 3352.
[10] F.B. Li, X.Z. Li, M.F. Hou, K.W. Cheah, W.C.H. Choy, Appl. Catal. A: Gen. 285 (2005) 181.
[11] Y. Zhang, H. Xu, Y. Xu, H. Zhang, Y. Wang, J. Photochem. Photobiol. A: Chem. 170 (2005) 279.
[12] X. Yan, J. He, D. Evans, X. Duan, Y. Zhu, Appl. Catal. B: Environ. 55 (2005) 243.
[13] Y. Xie, C. Yuan, X. Li, Mater. Sci. Eng. B 117 (2005) 325.
[14] J.C. Yu, J.G. Yu, K.W. Ho, Z.T. Jiang, L.Z. Zhang, Chem. Mater. 14 (2002) 3808.
[15] M. Anpo, N. Aikawa, Y. Kubokawa, M. Che, C. Louis, E. Giamello, J. Phys. Chem. 89 (1985) 5017.
[16] W.F. Zhang, M.S. Zhang, Z. Yin, Q. Chen, Appl. Phys. B 70 (2000) 261.
[17] L.Q. Jing, X.J. Sun, W.M. Cai, Z.L. Xu, Y.G. Du, H.G. Fu, J. Phys. Chem. Solids 64 (2003) 615.
[18] V. Kiisk, I. Sildos, S. Lange, V. Reedo, T. Tätte, M. Kirm, J. Aarik, Appl. Surf. Sci. 247 (2005) 412.
[19] C.C. Ting, S.Y. Chen, W.F. Hsieh, H.Y. Lee, J. Appl. Phys. 90 (2001) 5564.
[20] R. Palomino-Merino, A. Conde-Gallardo, et al., Thin Solid Films 401 (2001) 118.
[21] A. Conde-Gallardoa, M. Garcı′ a-Rocha, R. Palomino-Merino, M.P. Vela′squez-Quesada, I. Herna′ndez-Caldero′n, Appl. Surf. Sci. 212 (2003) 583.
[22] S. Lange, I. Sildos, V. Kiisk, J. Aarik, Mater. Sci. Eng. B 112 (2004) 87.
[23] V. Reedo, S. Lange, V. Kiisk, Proc. SPIE 5946 59460F-1.
[24] L.Q. Jing, B.F. Xin, F.L. Yuan, L.P. Xue, B.Q. Wang, H.G. Fu, J. Phys. Chem. B 110 (2006) 17860.
[25] S. Makishima, H. Yamamoto, T. Tomotsu, J. Phys. Soc. Jpn. 20 (1965) 2147.
[26] K.L. Frindell, M.H. Bartl, J. Solid State Chem. 172 (2003) 81.